Bone 122 (2019) 218–230

Contents lists available at ScienceDirect

Bone

journal homepage: www.elsevier.com/locate/bone

Full Length Article

GIT1 is critical for formation of the CD31^{hi}Emcn^{hi} vessel subtype in coupling osteogenesis with angiogenesis via modulating preosteoclasts secretion of PDGF-BB

Tao Xu[a,1], YongJun Luo[a,1], FanQi Kong[a,1], Bin Lv[b], ShuJie Zhao[a], Jian Chen[a], Wei Liu[a], Lin Cheng[a], Zheng Zhou[a], ZhiMin Zhou[a], YiFan Huang[a], LinWei Li[a], Xuan Zhao[a], DingFei Qian[a], Jin Fan[a,*], GuoYong Yin[a,*]

[a] Department of Orthopedic, the First Affiliated Hospital of Nanjing Medical University, 300 Guangzhou Rd., Nanjing 210029, China
[b] Department of Orthopedics, The Affiliated People's Hospital with Jiangsu University, Zhenjiang, Jiangsu Province 212000, China

ARTICLE INFO

Keywords:
GIT1
Endomucin
Bone formation
Endothelial cells
PDGF-BB
Preosteoclasts

ABSTRACT

G protein-coupled receptor kinase 2 interacting protein-1 (GIT1) is a scaffold protein that plays a vital role in bone modeling and remodeling during osteogenesis coupled with angiogenesis. Recent studies have shown that a specialized subset of vascular endothelium strongly positive for CD31 and Endomucin (CD31^{hi}Emcn^{hi}) is coupled with anabolic bone formation. Based on our previous finding that GIT1 knockout (GIT1 KO) mice have impaired angiogenesis and bone formation, we hypothesized that GIT1 affects formation of the CD31^{hi}Emcn^{hi} vessel subtype. In the current study, GIT1 knockout (GIT1 KO) mice displayed a significant decrease in trabecular bone mass and CD31^{hi}Emcn^{hi} vessel number, compared to their wild-type counterparts. In the fracture healing mouse model, GIT1 KO mice contained a lower number of CD31^{hi}Emcn^{hi} vessels in fracture callus at days 7 and 14. However, no significant differences in the number of preosteoclasts in bone marrow, trabecular bone and callus in GIT1 KO mice were observed, compared with wild-type mice. Notably, concentrations of serum platelet-derived growth factor-BB(PDGF-BB) secreted by preosteoclasts associated with CD31^{hi}Emcn^{hi} vessel formation were lower in GIT1 KO mice. In addition, PDGF-BB-associated expression of phosphorylated extracellular signal-regulated kinase- 1/2 (ERK1/2) and specificity protein 1 (SP1) was significantly decreased in preosteoclasts of GIT1 KO mice. These results collectively suggest that GIT1 is a critical participant in formation of the CD31^{hi}Emcn^{hi} vessel subtype, highlighting a novel biologic function of this scaffold protein in preosteoclasts.

1. Introduction

Bone modeling and remodeling are essential to ensure normal structure and integrity of the skeleton [1,2]. Several primary modulatory factors of these processes have been characterized to date [3,4]. Among these, angiogenesis is known to play a vital role in metabolism of bone [5,6]. During bone modeling and remodeling, endothelial cells invade cartilage at the growth plate region for nutrient supply and act as a scaffold for new bone formation [6,7]. Capillaries additionally play an important role in bone resorption and formation [7,8]. Migration and proliferation of endothelial cells, capillary formation and mesenchymal stem cells (MSCs) stabilization are involved in angiogenesis [9,10]. Recent studies have identified a specific vascular endothelium type during angiogenesis, CD31^{hi}Emcn^{hi}, that actively directs osteogenesis [11,12]. Platelet-derived growth factor-BB (PDGF-BB) is believed to induce migration and angiogenesis of endothelial progenitor cells (EPC) [13,14]. CD31^{hi}Emcn^{hi} endothelium levels are associated with concentrations of platelet-derived growth factor-BB (PDGF-BB) secreted by preosteoclasts (tartrate resistant acid phosphatase positive mononuclear cells) [15,16]. However, the mechanisms underlying cellular and molecular regulation of PDGF-BB secretion by preosteoclasts associated with CD31^{hi}Emcn^{hi} endothelium levels remain unclear at present.

G protein-coupled receptor kinase 2 interacting protein-1 (GIT1), a scaffold protein binding to GPCR kinase 2, is involved in adrenergic receptor endocytosis [17,18]. Previously, our group demonstrated that GIT1 is composed of five distinct structures, including an ADP-ribosylation factor GTPase-activating protein (ARF-GAP) domain, a Spa

* Corresponding authors.
E-mail addresses: fanjin@njmu.edu.cn (J. Fan), guoyong_yin@sina.com (G. Yin).
[1] These authors contributed equally to this work.

https://doi.org/10.1016/j.bone.2019.03.006
Received 25 December 2018; Received in revised form 6 March 2019; Accepted 6 March 2019
Available online 07 March 2019
8756-3282/

homology domain, three ankyrin repeats, a synaptic localization domain and a conserved paxillin-binding site [19]. Through these domains, GIT1 interacts with multiple signal molecules to exert a wide range of biological effects [20]. GIT1 participates in pulmonary vascular development through modulation of VEGF-induced PLCγ and ERK1/2 activation [21]. GIT1 is additionally known to regulate endothelial cell (EC) and VSMC migration [22]. In terms of bone homeostasis and the skeletal system, GIT1 plays a physiological role in maintenance of bone mass by OC [23]. GIT1 additionally affects fracture healing and vascular formation in a fracture healing mouse model [24]. Given its critical role in angiogenesis and osteoclast functions, both of which are related to $CD31^{hi}Emcn^{hi}$ endothelium, we hypothesize that GIT1 influences osteogenesis through effects on the formation of $CD31^{hi}Emcn^{hi}$ endothelium.

In the current study, we have demonstrated that knockdown of GIT1 induces loss of bone mass accompanied by a decrease in $CD31^{hi}Emcn^{hi}$ skeletal vessels. Abundant $CD31^{hi}Emcn^{hi}$ endothelium was observed in bone callus during the fracture healing process, which was decreased upon deletion of GIT1. We observed no significant differences in the number of preosteoclasts in bone marrow and in vitro culture between GIT1 KO and GIT1 WT mice although a decrease in serum PDGF-BB secretion by preosteoclasts of GIT1 KO mice was evident. Additionally, GIT1 was identified as an endogenous regulator of ERK1/2 phosphorylation, leading to activation of nuclear SP1, which is essential for expression of PDGF-BB that induces formation of the $CD31^{hi}Emcn^{hi}$ vessel subtype for coupling osteogenesis with angiogenesis.

2. Materials and methods

2.1. Animals

Homozygous GIT1 knockout mice (C57BL/6 background) were obtained from Bradford C. Berk (University of Rochester, Cardiovascular Research Institute) and GIT1 KO mice generated in the laboratory (Aab Cardiovascular Research Institute and Department of Medicine, University of Rochester, Rochester, NY, USA) as described previously [21]. Wild-type littermates (GIT1 WT) were used as the control group. Genotypes of mice were determined via RT-PCR analysis of genomic DNA samples isolated from mouse tails. All animals were maintained in the Animal Facility of the First Affiliated Hospital of Nanjing Medical University. The experimental protocol was reviewed and approved by the Animal Committee at the First Affiliated Hospital of Nanjing Medical University (Nanjing, China).

2.2. MicroCT analysis

Femora were dissected from mice, fixed overnight in 70% ethanol and analyzed via high-resolution microcomputed tomography imaging (MicroCT) (Skyscan 1172, Skyscan) [25–27]. Image reconstruction (NRecon v1.6), data analysis (CTAn v1.9) and three-dimensional model visualization (μCTVol v2.0) software were employed to analyze parameters of distal femoral metaphyseal trabecular bone and callus volume [28–30]. The region of interest of trabecular bone and bone callus has been described previously [15,23,24]. The parameters for assessment include trabecular bone volume fraction (BV/TV), trabecular thickness (Tb. Th), trabecular number (Tb. N), trabecular separation (Tb. Sp), trabecular pattern factor (Tb. Pf) and bone mineral density (BMD) [15].

2.3. Mouse femur fracture model

A femoral fracture mouse model was generated according to previous reports [24,31]. All surgical procedures were performed under isoflurane (1%–4%) anesthesia via nosecone. After anesthesia and surgical site sterilization, skin and underlying tissues above the right anterolateral femur were incised. Femur and patella were exposed and a 25-gauge needle inserted through the patellar tendon and into the marrow cavity. A single cut was made in the middle of the femoral diaphysis via three-point bending using an Einhorn device [24,32]. The wound was stitched with absorbable lines. Following surgery, prophylactic antibiotics and painkillers were used every 3 days.

2.4. Immunocytochemistry and immunofluorescence

For immunocytochemical staining, cultured preosteoclasts were incubated with a primary antibody against PDGF-BB (Abcam) for 2 h at 37 °C and immunoreactivity detected using a horseradish peroxidase–streptavidin system (Dako).

After euthanasia, femora were dissected, fixed with intact periosteum in 10% buffered formalin for 48 h and decalcified in 10% EDTA (pH 7.4) for 21 days. Next, samples were embedded in paraffin or optimal cutting temperature compound.

For immunofluorescence staining, bone slices and cultured cells were obtained as described previously [27,33,34]. Briefly, after treatment with Triton X-100 PBS solution (0.3%, w/v) for 10 min, samples were blocked with goat serum PBS solution (10%, v/v) at room temperature for 30 min and incubated overnight at 4 °C with the following primary antibodies: CD31 (1:50, Abcam), Endomucin (1:50, Santa Cruz) and SP1 (1:500, Abcam). Samples were subsequently incubated with secondary antibodies at room temperature for 1 h in the absence of light. Nuclei were stained with DAPI and fluorescent images acquired. Quantitative analysis of fluorescent images was performed according to earlier reports [15,31,33]. In brief, the numbers or areas of positively stained cells in distal metaphysis or bone callus per femur in five sequential sections per mouse in each group were calculated using ImageJ software.

A TRAP staining kit (Sigma Aldrich) was used on bone slices and cultured cells as described previously [15,31,33].

2.5. Flow cytometry

For analysis or sorting of $CD31^{hi}Emcn^{hi}$ endothelial cells, femora and tibiae were collected from 4 week-old male mice. Epiphysis at the end and muscle around the bone were removed and metaphysis and diaphysis regions of bone crushed in ice-cold PBS. To obtain a single cell suspension, whole bone marrow was digested with collagenase for 20 min at 37 °C. Equal numbers of cells were incubated for 45 min at 4 °C with Endomucin antibody (eBioscience, 50-5851-80), washed, and further incubated with CD31 antibody (Miltenyi Biotec, 130102-608).

For analysis or sorting of preosteoclasts in bone, femora and tibiae were processed as described above to obtain single cell suspensions, which were subsequently labeled with antibodies against CD11b (Miltenyi Biotec, 130109-363) and Gr-1 (Miltenyi Biotec, 130-112-307) and sorted into CD11b + Gr-1low + med cells (the OCP subset) [35].

For analysis or sorting of bone marrow endothelial cells, the cell extraction method was performed as described above. Cells were incubated for 45 min at 4 °C with CD31 (Miltenyi Biotec, 130–102-608), CD45 (Biolegend, 30-F11) and Ter119 (Biolegend, TER-119) and sorted as CD31 + CD45 − Ter119 − cells [15].

All samples were analyzed on a flow cytometer (BD Biosciences, San Jose, CA, USA) and data evaluated using FlowJo software (Tree Star, Ashland, OR, USA).

2.6. Preosteoclasts and osteoclast (OC) cultures

Monocytes/macrophages were harvested from bone marrow of 4 week-old male mice by flushing femur and tibia. Flushed bone marrow cells were cultured overnight on petridishes in α-MEM containing 10% FBS, 100 U ml^{-1} penicillin, 100 μg ml^{-1} streptomycin sulfate and 30 ng ml^{-1} M-CSF (R&D Systems). Nonadherent cells were incubated with M-CSF (30 ng ml^{-1}) to obtain pure monocytes/macrophages. Upon incubation of monocytes/macrophages in 24-well plates (1×10^5 cells per well) with 30 ng ml^{-1} M-CSF and 60 ng ml^{-1} RANKL

(R&D Systems), all cells became preosteoclasts after 3–4 days of culture. Alternatively, fully mature multinucleated osteoclasts were formed after incubation with 30 ng ml^{-1} M-CSF and 60 ng ml^{-1} RANKL (R&D Systems) for 8 days. TRAP activities of the cultured preosteoclasts and OCs were assessed via staining using a commercial kit (Sigma-Aldrich). During induction, conditioned medium was harvested from preosteoclasts and mature osteoclasts. Serum-free conditioned medium was harvested after one-day culture with serum-free medium containing the same concentrations of M-CSF and RANKL. After centrifugation (2500 ×g for 10 min at 4 °C), conditioned medium was stored at −80 °C.

2.7. ELISA

PDGF-BB analysis of conditioned medium was performed using a mouse PDGF-BB Quantikine ELISA kit (R&D Systems). All assays were conducted according to the manufacturer's instructions.

2.8. Real-time PCR

Cultured preosteoclasts at different time-points were treated with TRIzol (Invitrogen) and mRNA purified according to the TRIzol System protocol. Reverse transcriptase reactions were performed using an iScript™ cDNA Synthesis kit (Bio-Rad). All primers are listed in Table 1. cDNA was amplified using the IQ™ SYBR® Green Supermix (Bio-Rad) on an Applied Biosystems 7900 Real-Time PCR system. Each sample was analyzed in triplicate. Target genes were normalized to the reference housekeeping gene, glyceraldehyde-3-phosphate dehydrogenase (GAPDH), and relative expression levels determined based on normalized CT values.

2.9. EPC culture

Late-stage endothelial progenitor cells (EPC) isolated from bone marrow of 8 week-old C57BL/6 mice were obtained from BioChain (7030031) as described previously [13,31]. These cells display spindle morphology and express a variety of endothelial cell markers such as CD31, CD105, vascular endothelial growth factor receptor 1 and neuropilin-1 but are negative for CD133.

2.10. Migration assay

Cell migration was assessed in Transwell-96 well plates (Corning) with 8 μm pore filters. In brief, EPCs were seeded at a concentration of 1 × 10^4/well in the upper chambers, then incubated them with conditioned medium from preosteoclasts and osteoclasts in the lower chambers for 4 h. At the same time, vehicle or neutralizing antibody for PDGF-BB (Abcam) were also added to the lower chamber. Subsequently, cells were fixed with 10% formaldehyde for 30 min and cells of each filter on the surface of upper chambers removed with cotton swabs. Cell that migrated through the pores to the lower surface were stained with crystal violet (Sigma-Aldrich) and quantified by counting three random fields per well using an optical microscope.

To assess migration ability, the scratch wound assay was performed as described previously [36]. Briefly, EPCs were seeded into six-well plates at a density of 2 × 10^5 cells/well and grown to 80% confluence. Next, confluent layers of cells were scratched using a sterile pipette tip. After washing, conditioned medium was added as described above. Images were recorded at 0 h and12 h after scratching.

Table 1
Primer sequence.

Name	Sequence
mus-GIT1-1F	**CCTGGGACGACACATCTCC**
mus-GIT1-1R	**GATGGGGTGGACTTTATCTTGG**
mus-PDGF-B -F	**CATCCGCTCCTTTGATGATCTT**
mus-PDGF-B-R	**GTGCTCGGGTCATGTTCAAGT**
mus-GAPDH-F	**GGTGAAGGTCGGTGTGAACG**
mus-GAPDH-R	CTCGCTCCTGGAAGATGGTG

Mouse G protein-coupled receptor kinase 2 interacting protein-1(mus-GIT1) primer sequences, mouse Platelet-derived growth factor-B chain (mus-PDGF-B) primer sequences, mouse glyceraldehyde-3-phosphate dehydrogenase (mus-GAPDH) primer sequences.

2.11. Tube formation assay

Matrigel (BD Biosciences) was plated on 96-well culture plates and incubated for 45 min at 37 °C to allow polymerization. EPCs were seeded at a density of 2.0 × 10^4 cells/well in Matrigel-coated plates and cultured with serum-free conditioned medium collected from preosteoclasts cell culture systems. After incubation for 4 h at 37 °C, tube formation was observed via microscopy and measured based on cumulative tube length. In specific experiments, the neutralizing antibody for PDGF-BB was added to preosteoclasts conditioned medium.

2.12. Western blot analysis

Proteins were extracted from cells using RIPA lysis and Extraction buffer (KeyGen Biotechnology) and protein concentrations detected using the Bradford method. Equal amounts of protein were separated via sodium dodecyl sulfate polyacrylamide gel electrophoresis, transferred to polyvinylidene difluoride membranes (Millipore) and incubated overnight at 4 °C with primary Abs, followed by blocking with bovine serum albumin (5%, v/v). The primary antibodies used were specific for GIT1 (1:1000, Abcam), SP1 (1:1000, Abcam), ERK1/2 (1:1000, Cell Signaling), p-ERK1/2 (1:1000, Cell Signaling), GAPDH (1:1000, Abcam) and H3 (1:1000, Cell Signaling). Next, membranes were incubated at room temperature for 120 min with the appropriate secondary antibody (1:2000; Thermo Fisher Scientific). Immunoreactive bands were visualized using enhanced chemiluminescence (ECL) reagents (Thermo Fisher Scientific) and the density of protein bands semi-quantified using ImageJ (National Institutes of Health, Bethesda, MD, USA).

2.13. Plasmid transfection and luciferase activity assays

SP1 is reported to bind to the PDGF-B promoter and activate its transcription and translation [37,38]. Platelet Derived Growth Factor-B promoter–luciferase reporter (PDGF-BLUC) and SP1 overexpression plasmid were purchased from Obio Technology (Shanghai, China). HEK293T cells were seeded at a concentration of 8000 cells each well in 96-well plates and plasmid transfection performed with Lipofectamine®2000 reagent (Invitrogen). After 24–48 h, luciferase activity in transfected cells was measured with a Dual Luciferase Reporter Assay System (Promega, Madison, Wisconsin, USA). Normalized data were calculated as the quotient of Renilla/firefly luciferase activities (Rluc/FLuc). All assays were performed in triplicate and repeated three times.

2.14. Chromatin immunoprecipitation (CHIP) assay

Cells were treated with 1% formaldehyde to cross-link proteins to DNA. Cells were incubated in lysis buffer (150 mM NaCl, 25 mM Tris pH 7.5, 1% Triton X-100, 0.1% SDS, 0.5% deoxycholate) and treated with protease inhibitors. DNA of cell lysates was sheared into 300–500 bp segments using a Bioruptor PICO sonicator (DIAGENODE). Aliquots containing equal amounts of chromatin supernatants and 200 μg protein were used for immunoprecipitation reactions with anti-SP1 (Abcam) or anti-IgG antibody. After reverse cross-linking of protein-DNA complexes to free DNA, RT-PCR was conducted using primer sequences specific for the PDGF-B promoter (Forward:5′-CCCGATGCC TGTTTAGATGA-3′ and Reverse: 5′-AACCTCTCGGGCCTCTTTAC-3′).

2.15. Statistical analyses

All data are presented as means ± SD of at least three independent experiments. Two-tailed Student's.

t-test was used for comparisons between two groups and One-Way Analysis of Variance (ANOVA) with Bonferroni post hoc test for multiple comparisons. GraphPad PRISM software (v6.0a; GraphPad) was employed for statistical analysis. P values < 0.05 were considered statistically significant ($^{*}P < 0.05$; $^{**}P < 0.01$; $^{***}P < 0.001$).

3. Results

3.1. GIT1 KO mice have lower levels of $CD31^{hi}Emcn^{hi}$ endothelium

Previous research by our group disclosed a close association of Git1 with bone formation [23,24]. To test our hypothesis that GIT1 causes changes in bone mass by affecting $CD31^{hi}Emcn^{hi}$ endothelium formation , we harvested femora of 4 week-old male GIT1 WT and KO mice for three-dimensional microstructural analyses using high-resolution MicroCT, considering the influence of age on $CD31^{hi}Emcn^{hi}$ endothelium [11,12,39]. MicroCT analyses revealed decreased trabecular bone mass in GIT1 KO, compared to WT mice (Fig. 1A). Reduction of the percentage (%) of bone volume BV/TV% and Tb.Th was significant in GIT1 KO mice relative to their WT littermates. Tb.N and BMD were not significantly reduced in GIT1 KO mice, but showed a decreasing trend. Significant increase of Tb.Pf and Tb.Sp in GIT1 KO mice also indicate decreased trabecular bone mass in GIT1 KO, compared to WT mice (Fig. 1B). Previous studies have shown that angiogenesis, especially involving $CD31^{hi}Emcn^{hi}$ vessels, is closely related to formation of bone mass. Moreover, GIT1 is an important influencing factor of angiogenesis [21,22,40]. CD31 and Endomucin double-positive endothelium has been identified in marrow immediately beneath the growth plate [11,15,31]. In the current study Co-immunostaining of CD31 and Endomucin revealed significantly lower levels of $CD31^{hi}Emcn^{hi}$ vessels in marrow immediately beneath the growth plate in GIT1 KO mice relative to their wild-type littermates (Fig. 1C D). Flow cytometry analysis of $CD31^{hi}Emcn^{hi}$ endothelium similarly disclosed markedly lower levels of this subset of endothelial cells in GIT1 KO mice, compared to WT littermate controls (Fig. 1E). Taken together, our results suggest that GIT1 participates in fine-tuning the $CD31^{hi}Emcn^{hi}$ endothelium level in bone.

2、Association between GIT1 and $CD31^{hi}Emcn^{hi}$ vessels is essential for fracture healing.

Given that fracture healing is closely related to new blood vessel formation [41,42], we hypothesized that the connection between GIT1 and $CD31^{hi}Emcn^{hi}$ vessels is vital for bone repair. To examine this theory, an open femoral fracture model was established for analysis of fracture healing in GIT1 KO and WT control mice and the healing process evaluated via micro computed tomography (MicroCT) analysis of mineralized callus volume. At 14 days and 21 days post-fracture, healing appeared impaired in GIT1 KO mice according to quantification of mineralized callus volume (Fig. 2A B). Furthermore, immunofluorescence staining of CD31 and Endomucin at bone fracture callus showed abundant formation of $CD31^{hi}Emcn^{hi}$ endothelium in mice, clearly indicating that bone fracture healing is associated with formation of $CD31^{hi}Emcn^{hi}$ endothelium. Notably, the number of $CD31^{hi}Emcn^{hi}$ vessels at the fracture callus in GIT1 KO mice was significantly lower than that in wild-type littermates (Fig. 2,C,D). In view of these findings, we conclude that associations between GIT1 and $CD31^{hi}Emcn^{hi}$ vessels are essential for fracture healing.

3.2. GIT1 KO mice contain normal preosteoclasts levels

The decreased $CD31^{hi}Emcn^{hi}$ vessel number in GIT1 KO mice could be a consequence of either a decrease in the number of preosteoclasts or impairment of preosteoclasts function [15]. To clarify the underlying reason for this phenomenon, cultured cells from GIT1 KO and WT mice were stained at different time-points during osteoclastogenesis (OC differentiation) using the tartrate-resistant acid phosphotase (TRAP) assay [43] (Fig. 3A). Quantitative analysis of preosteoclasts and osteoclasts (OC) revealed comparable preosteoclasts and OC numbers between GIT1 KO mice and WT littermates in vitro (Fig. 3B). Flow cytometry analysis further confirmed similar amounts of preosteoclasts in bones of GIT1 KO and WT littermate control mice (Fig. 3C) [35], consistent with TRAP staining of femur sections (Fig. 3D). In addition, no differences in the preosteoclasts number at bone fracture callus of GIT1 KO and WT mice were evident (Fig. 4E). Our findings suggest that impaired function of preosteoclasts underlies the decrease in $CD31^{hi}Emcn^{hi}$ vessel number in GIT1 KO mice.

3.3. PDGF-BB secreted by preosteoclasts is reduced in GIT1 KO mice

Previous studies have reported that PDGF-BB secreted by preosteoclasts is crucial for $CD31^{hi}Emcn^{hi}$ vessel formation [15,44]. Therefore, we explored the possibility that GIT1affects the secretory function of preosteoclasts, which would lead to a decrease in $CD31^{hi}Emcn^{hi}$ vessel formation. To this end, we collected conditioned media of monocytes/macrophages, preosteoclasts and osteoclasts from GIT1 KO and WT mice for examining PDGF-BB secretion. ELISA analysis confirmed that preosteoclasts secrete high levels of PDGF-BB whereas osteoclasts display significantly lower secretion of PDGF-BB in both GIT1 KO and WT mice (Fig. 4A). Furthermore, at different time-points during osteoclastogenesis, ELISA of conditioned media samples of cultured cells showed significantly lower PDGF-BB secretion by GIT1 KO mice than WT littermate controls (Fig. 4B). PDGF- BB mRNA expression in cultured cells from GIT1 KO mice was reduced, compared with cells from WT littermate controls at different time-points during osteoclastogenesis (Fig. 4C). Consistently, immunohistochemical staining of preosteoclasts demonstrated higher abundance of PDGF-BB-positive cells in WT mice (Fig. 4D). Taken together, our data suggest that GIT1 affects the secretion of PDGF-BB in preosteoclasts associated with $CD31^{hi}Emcn^{hi}$ vessels.

3.4. Suppression of PDGF-BB secretion from preosteoclasts in GIT1 KO mice impairs migration and tube formation of EPC

PDGF-BB induces migration and angiogenesis of endothelial progenitor cells (EPC) [13]. To investigate the effects of reduction of PDGF-BB from preosteoclasts of GIT1 KO mice on EPC function, we collected conditioned media of preosteoclasts cultured from both GIT1 KO and WT mice. Interestingly, conditioned medium from GIT1 KO mice induced significantly lower EPC migration relative to that from GIT1 WT mice in a Transwell assay. Moreover, EPCs treated with recombinant PDGF-BB displayed enhanced migration in the GIT1 KO group and the PDGF-BB neutralizing antibody inhibited migration induced by conditioned medium of GIT1 WT preosteoclasts (Fig. 5A). Data from scratch wound assays confirmed the effect of reduced secretion of PDGF-BB from preosteoclasts of GIT1 KO mice on EPC migration (Fig. 5B).

Co-culture with conditioned medium of GIT1 KO preosteoclasts significantly attenuated EPC tube formation, compared with that in the GIT1 WT group. In addition, recombinant PDGF-BB enhanced EPC tube formation in the GIT1 KO group and a PDGF-BB neutralizing antibody attenuated tube formation in the GIT1 WT group (Fig. 5C). These results indicate that the decrease in PDGF-BB secretion from preosteoclasts of GIT1 KO mice leads to impairment of migration and tube formation of EPCs.

3.5. GIT1 modulates PDGF-BB secreted by preosteoclasts via SP1

To examine the molecular mechanism by which GIT1 affects PDGF-BB secreted by preosteoclasts, we prepared BM monocytes/macrophages and preosteoclasts induced on days 2 and 4 from GIT1 KO and

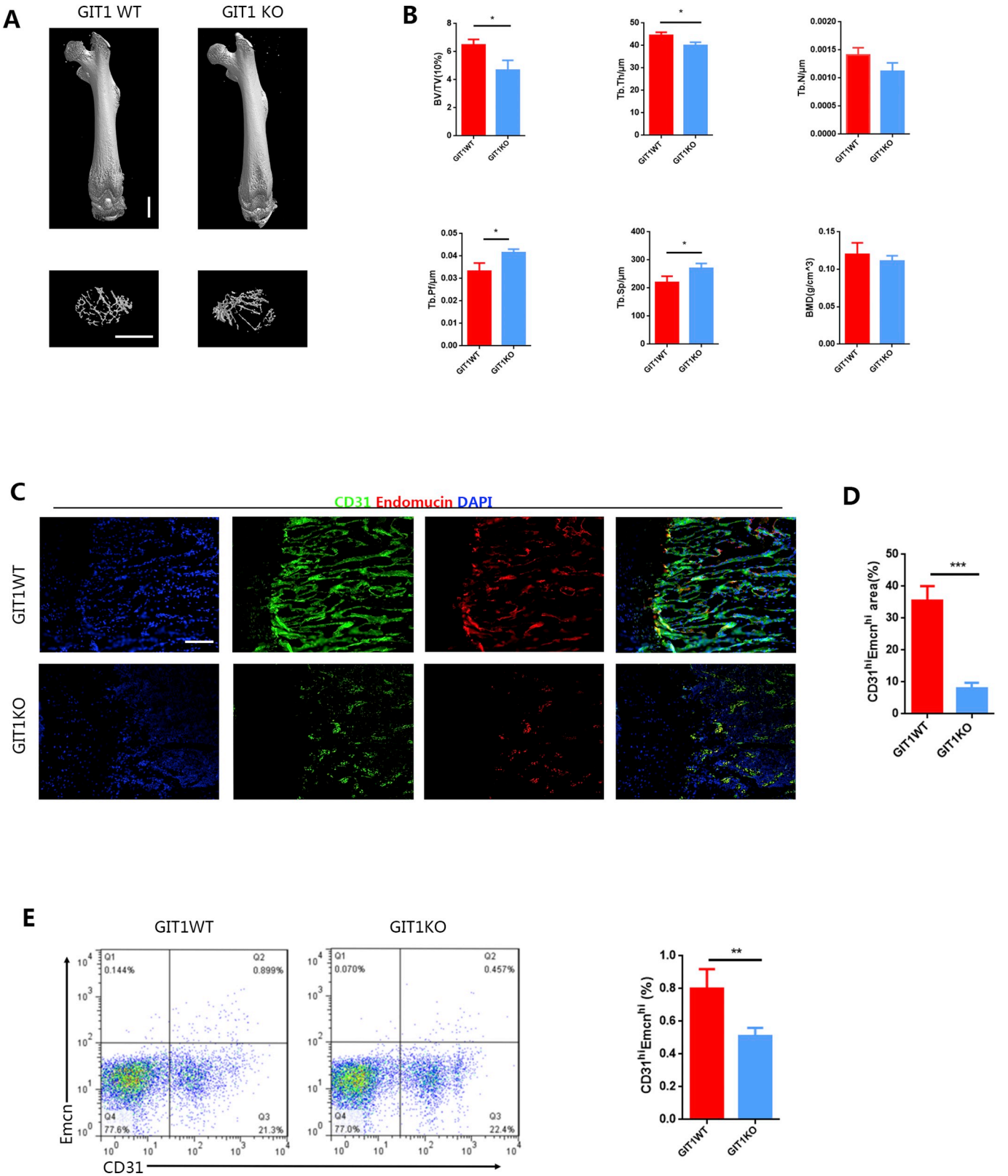

Fig. 1. Git1 regulates CD31hiEmcnhi endothelium associated with osteogenesis.

A. Representative Micro CT images of the trabecular bone in the distal femur metaphysis of 4-week-old GIT1 KO and GIT1 WT male mice. Scale bar, 1 mm.

B. Relative trabecular bone volume fraction (BV/TV), trabecular thickness (Tb. Th), trabecular number (Tb. N), trabecular separation (Tb. Sp), Trabecular pattern factor (Tb. Pf) and Bone Mineral Density (BMD) are shown ($n = 3$, $^{*}p < 0.05$, Student's *t*-test).

C. Fluorescent images of 4-week-old GIT1 KO and GIT1 WT male mice femurs stained with CD31 (green), Emcn (red) and DAPI (blue). Scale bars, 200 μm.

D. Quantification analysis of relative CD31hiEmcnhi(yellow) vessel area of the femur sections in 4-week-old GIT1 KO and GIT1 WT male mice ($n = 4$, $^{***}P < 0.001$, Student's *t*-test).

E. Flow cytometry plots (left) and relative percentage (right) of CD31hiEmcnhi cells in total bone marrow cells (BMCs) from 4-week-old GIT1 KO and GIT1 WT male mice (n = 4, $^{**}P < 0.01$, Student's *t*-test). (For interpretation of the references to colour in this figure legend, the reader is referred to the web version of this article.)

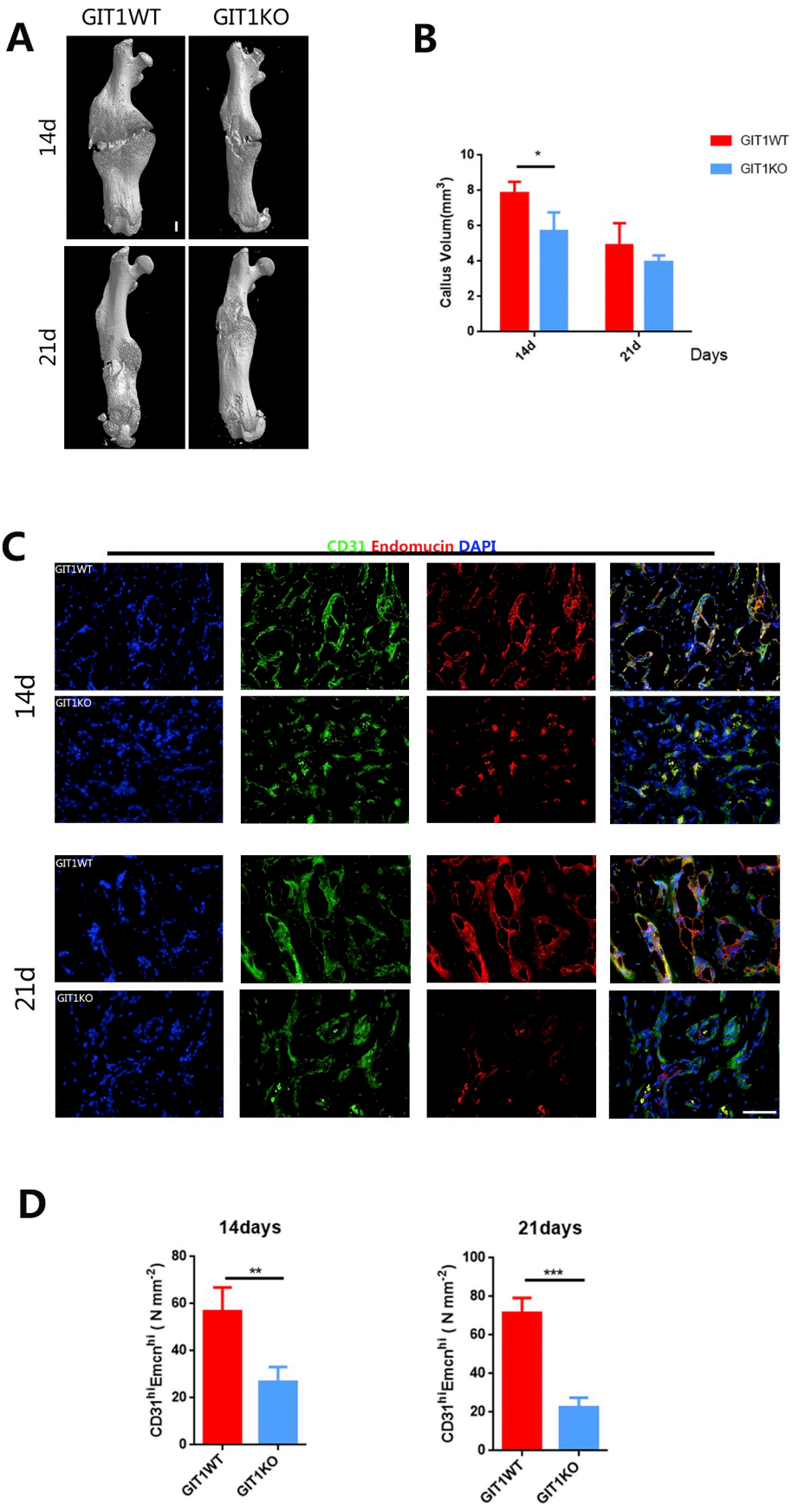

Fig. 2. The effect of the association between GIT1 and CD31hiEmcnhi vessels on fracture healing

A. Representative Micro CT images of mouse femurs 14 and 21 days after femoral fracture. Scale bars, 1 mm.

B. Quantification of bone callus volume of the fractured femora 14 and 21 days after fracture between GIT1 KO and GIT1 WT male mice ($n = 4$, *p $<$ 0.05, Student's *t*-test).

C. Fluorescent images of CD31hiEmcnhi cells (yellow) in callus sections of mouse femurs 21 days after fracture. Scale bars, 50 μm.

D. Quantification analysis of the number of CD31hiEmcnhi cells in callus sections of GIT1 KO and GIT1 WT male mouse femurs 14 and 21 days after fracture ($n = 4$, **P $<$ 0.01, ***P $<$ 0.001, Student's *t*-test). (For interpretation of the references to colour in this figure legend, the reader is referred to the web version of this article.)

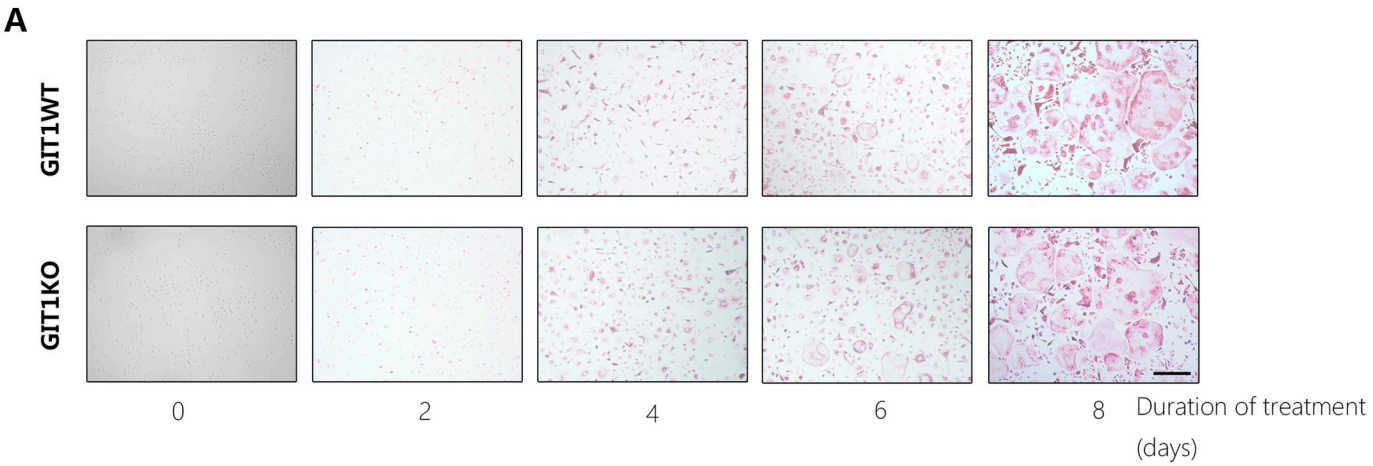

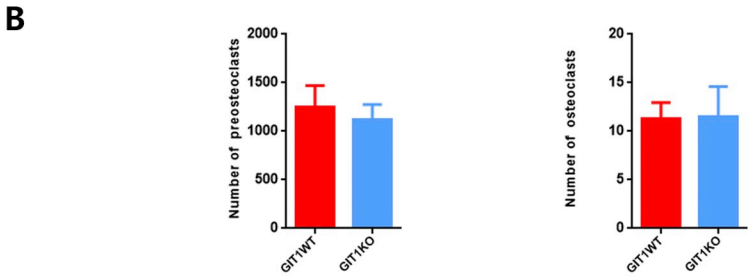

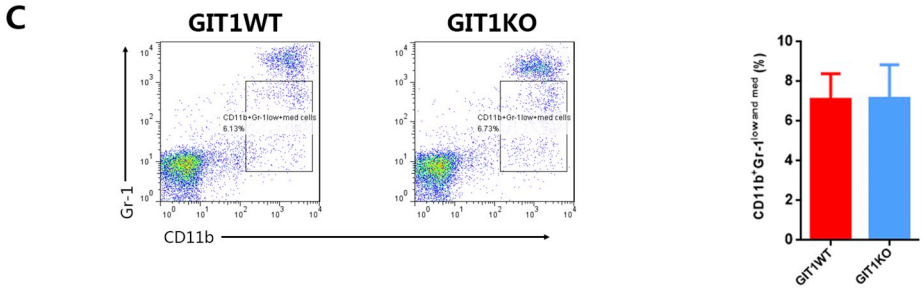

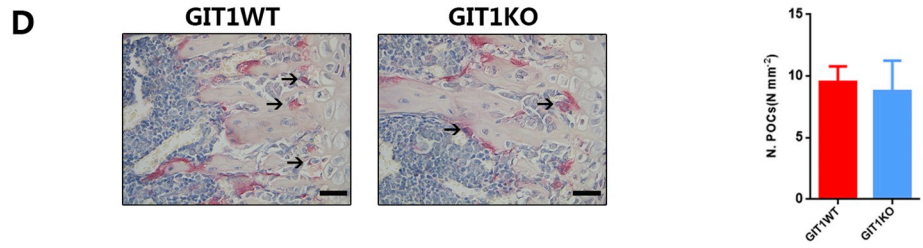

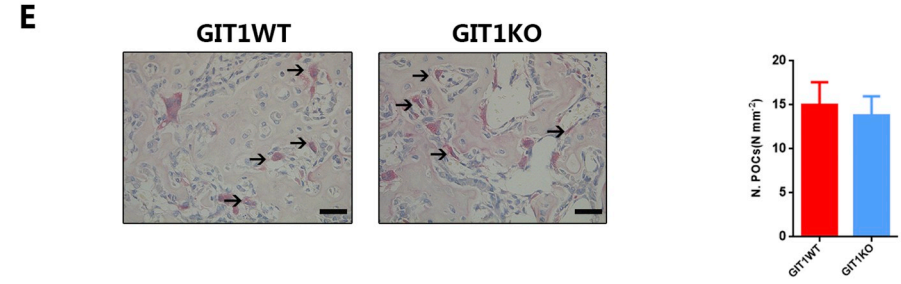

(caption on next page)

Fig. 3. Knocking out GIT1 has no effect on preosteoclasts levels in vitro or in vivo.
A. TRAP staining images of cells treated with M-CSF and RANKL for different days for the development of different stages of TRAP+ cells. Scale bars, 200 μm.
B. Quantitative analysis of the number of preosteoclasts on the fourth day and the number of osteoclasts on the eighth day ($n = 5$, No significant, Student's *t*-test).
C. Flow cytometry dot plots (left) and relative percentage (right) of CD11b + Gr-1low + med cells (the OCP subset) of the femur in 4-week-old GIT1 KO and GIT1 WT male mice ($n = 4$, No significant, Student's *t*-test).
D. TRAP staining images (left) and quantitative analysis of the number of preosteoclasts (N. POCs) (right) at the trabecular bone in the distal femur metaphysis of 4-week-old GIT1 KO and GIT1 WT male mice. Scale bars, 25 μm (n = 4, No significant, Student's *t*-test).
E. TRAP staining images (left) and quantitative analysis of the number of preosteoclasts (right) in callus sections of GIT1 KO and GIT1 WT male mouse femurs 14 days after fracture. Scale bars, 25 μm (n = 4, No significant, Student's *t*-test).

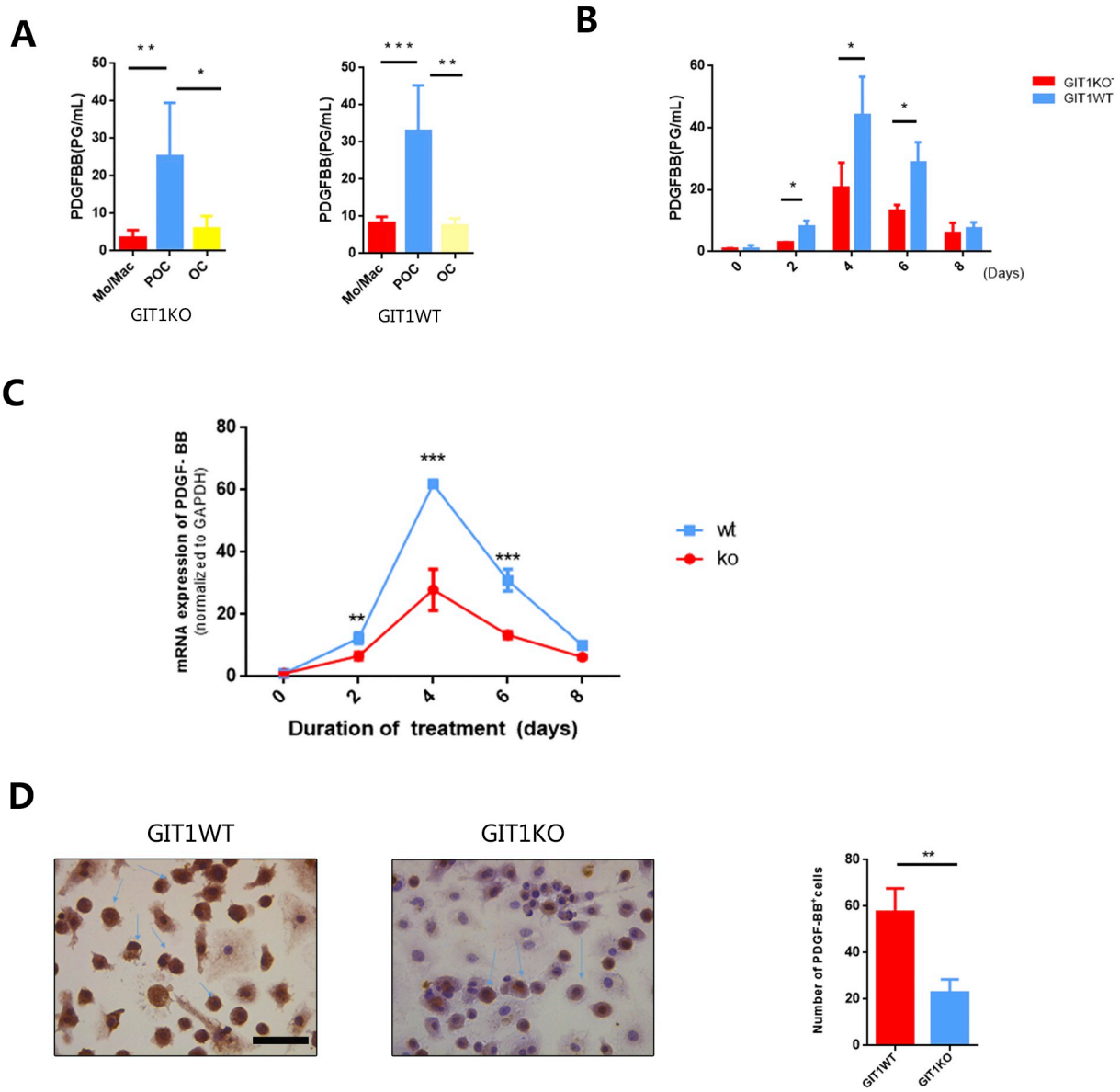

Fig. 4. Preosteoclasts have lower PDGF-BB expression levels in GIT1 KO mice.
A. ELISA analysis of concentrations of PDGF-BB in conditioned media (CM) of monocytes/macrophages (Mo/Mac), preosteoclasts(POC) and osteoclasts(OC) from GIT1 KO and WT mice ($n = 6$, $^{*}p < 0.05$, $^{**}P < 0.01$, $^{***}P < 0.001$, one-way ANOVA).
B. ELISA analysis of concentrations of PDGF-BB of GIT1 KO and WT cells treated with M-CSF and RANKL for different days for the development of different stages of TRAP+ cells (n = 6, $^{*}p < 0.05$, Student's *t*-test).
C. Quantification analysis of the mRNA expression of PDGF- BB in cultured cells of GIT1 KO and WT mice at different time points during osteoclastogenesis ($n = 3$, $^{**}P < 0.01$, $^{***}P < 0.001$, one-way ANOVA).
D. In vitro cultured preosteoclasts of GIT1 KO and WT mice were stained for PDGF-BB (brown) (left) and quantitative analysis of the number of PDGF-BB positive cells (right). Scale bars, 25 μm (n = 3, $^{*}p < 0.05$, Student's t-test). (For interpretation of the references to colour in this figure legend, the reader is referred to the web version of this article.)

WT mice. GIT1 is closely related to phosphorylation of ERK1/2 [45]. ERK1/2 phosphorylation further enhances expression and nuclear import of SP1, resulting in increased PDGF-B gene expression. Data from our western blot analysis showed that expression of GIT1,

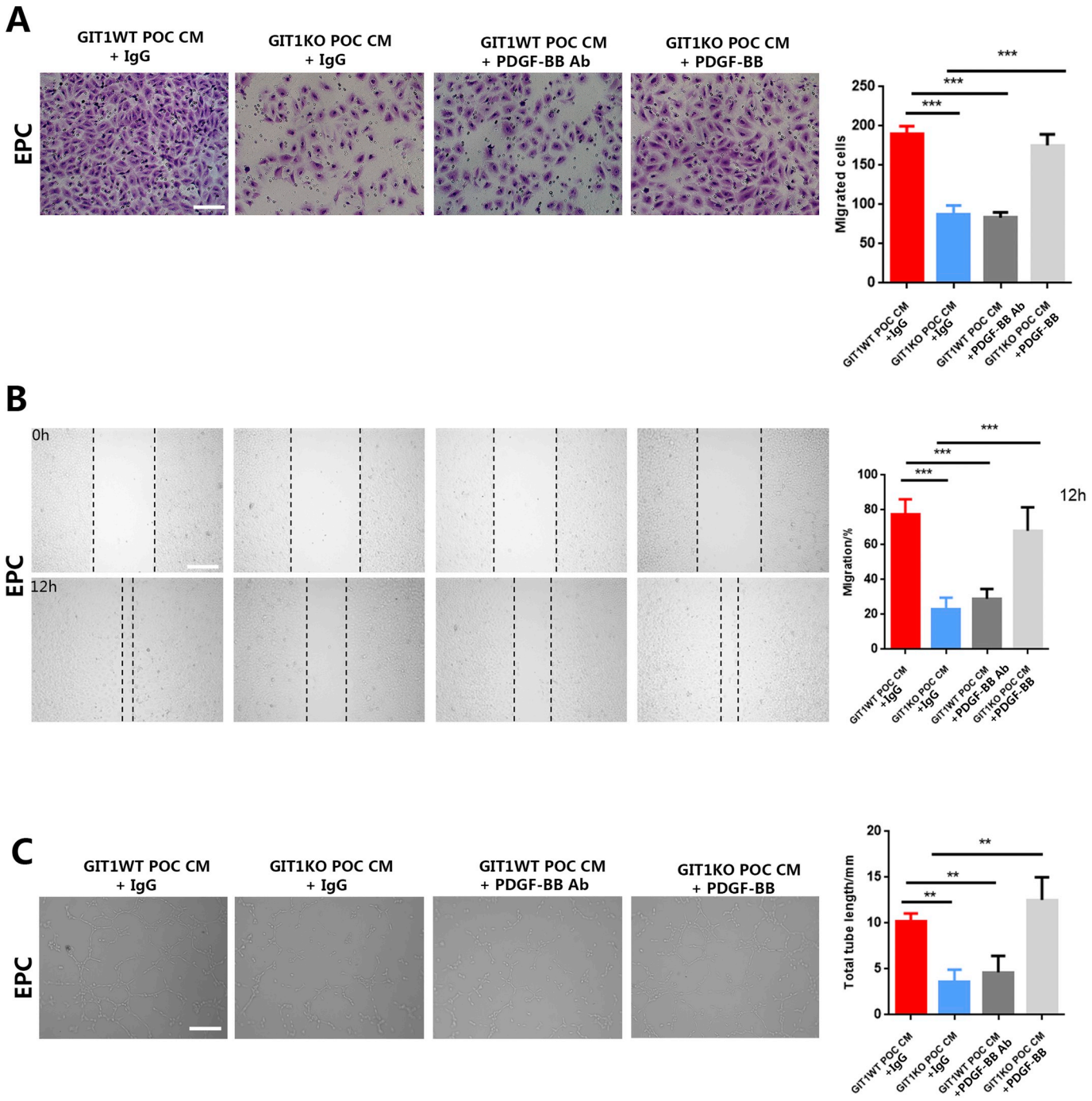

Fig. 5. Suppression of PDGF-BB in GIT1 KO preosteoclast conditioned medium impairs migration and tube formation of EPC.
A. Transwell assay images (left) and quantitative analysis of the migration of EPC after incubation using GIT1 KO and WT preosteoclast (POC) conditioned medium (CM) with addition of neutralizing PDGF-BB antibody, recombinant PDGF-BB or IgG for 24 h (right). Scar bar, 100 μm (n = 4, ***P < 0.001, one-way ANOVA).
B. Scratch wound assay images (left) and quantitative analysis of the migration ability of EPC using GIT1 KO and WT preosteoclast (POC) conditioned medium (CM) with addition of neutralizing PDGF-BB antibody, recombinant PDGF-BB or IgG at 0 h and 12 h (right). Scar bar, 100 μm (n = 4, ***P < 0.001, one-way ANOVA).
C. Tube formation assay images (left) and quantitative analysis of cumulative tube length with EPC using GIT1 KO and WT preosteoclast (POC) conditioned medium (CM) with addition of neutralizing PDGF-BB antibody, recombinant PDGF-BB or IgG (right). Scale bar, 100 μm (n = 4, **P < 0.01, one-way ANOVA).

phosphorylation of ERK1/2 and SP1 increased with preosteoclasts increase during the induction process, especially on day 4 when the number of preosteoclasts was maximal. Phosphorylation of ERK1/2 and SP1 in GIT1 knockout preosteoclasts was significantly decreased, in particular, on days 2 and 4 (Fig. 6 A B). In addition, the induced preosteoclasts contained higher levels of SP1 in the nucleus. The nuclear SP1 level of GIT1 knockout preosteoclasts was significantly reduced, compared to that of GIT1 wild-type preosteoclasts (Fig. 6 C D). Immunofluorescence staining also confirmed significantly lower SP1 in nuclei of GIT1 knockout preosteoclasts relative to GIT1 wild-type preosteoclasts (Fig. 6 E) Importantly, less SP1 was recruited to the PDGF-B promoter in GIT1 knockout preosteoclasts, as detected with the ChIP assay. Relative luciferase activity was significantly increased in HEK293T cells cotransfected with SP1 and PDGF-B. Both ChIP and luciferase assays showed that SP1 is recruited to the PDGF-B promoter and activates PDGF-B transcription, and GIT1 influences SP1 activity

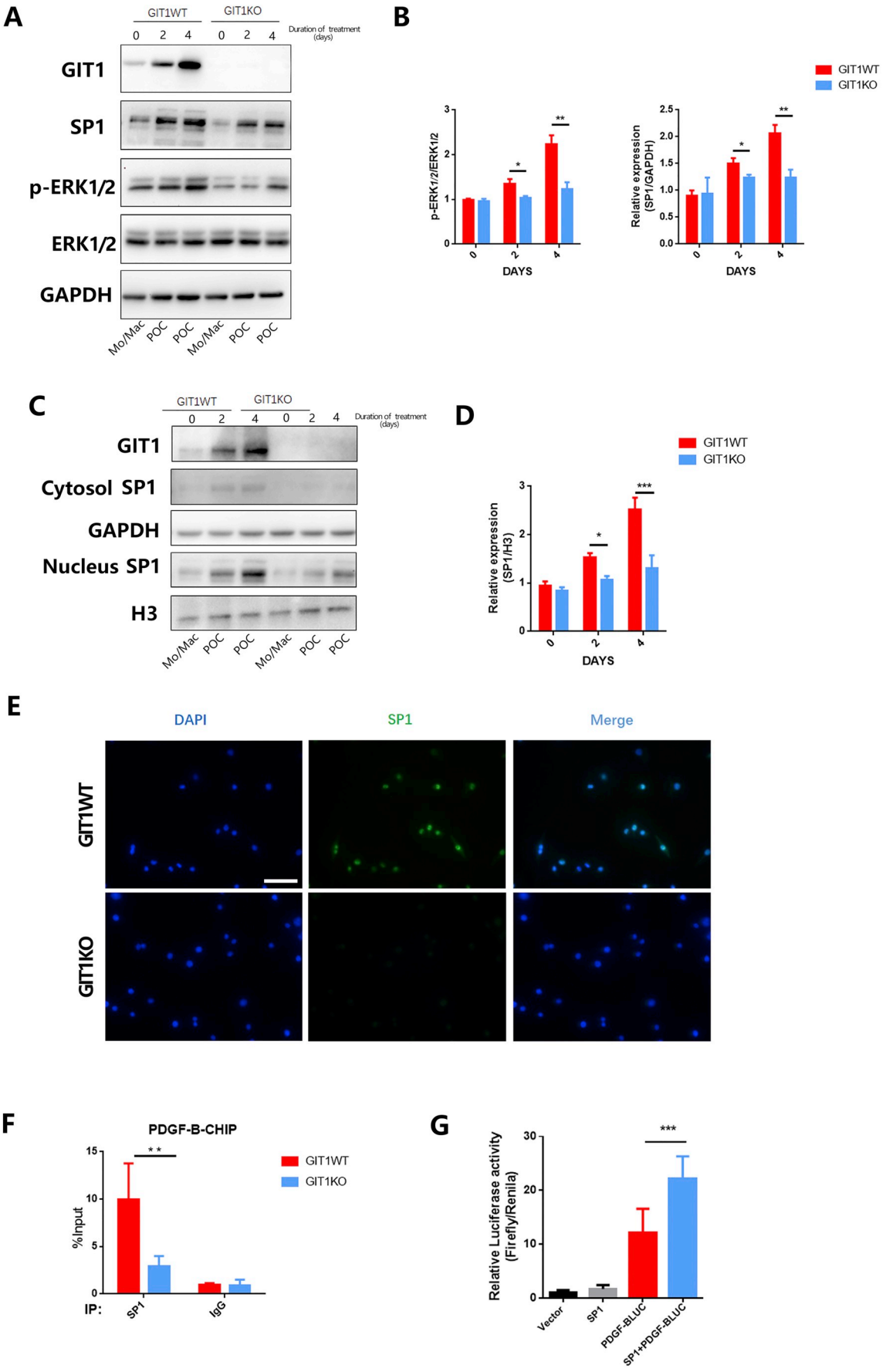

(caption on next page)

Fig. 6. GIT1 modulates PDGF-BB secreted by preosteoclasts via ERK1/2/SP1 signaling pathway.
A. Western blot of GIT1, SP1, ERK1/2 and phosphorylation of ERK1/2 in cultured monocytes/macrophages(Mo/Mac) and preosteoclasts(POC) from GIT1 KO and WT mice treated with M-CSF and RANKL for different days for the development of different stages of TRAP+ cells.
B. Quantitative analysis of the relative protein levels of cultured monocytes/macrophages and preosteoclasts. Glyceraldehyde 3-phosphate dehydrogenase (GAPDH) was used as loading control ($n = 3$, $^{*}p < 0.05$, $^{**}P < 0.01$, Student's *t*-test).
C. Western blot of SP1 translocation to the nucleus in cultured monocytes/macrophages (Mo/Mac) and preosteoclasts (POC) from GIT1 KO and WT mice inducted at the second and fourth days
D. Quantitative analysis of the relative SP1 levels in the cytoplasm and nucleus of cultured cells. Histone 3(H3) was used as loading control (n = 3, $^{*}p < 0.05$, $^{***}P < 0.001$, Student's *t*-test).
E. Fluorescent images of cultured preosteoclasts of GIT1 KO and WT mice were stained with SP1 (green) and DAPI (blue) in vitro. Scale bars, 50 μm.
F. Recruitment of SP1 to the PDGF-B promoter was assessed by ChIP assay with the indicated antibodies ($n = 6$, $^{**}P < 0.01$, Student's *t*-test).
G. Transcriptional activation of PDGF-B by SP1 was assessed with the luciferase assay (n = 6, $^{***}P < 0.001$, Student's *t*-test). (For interpretation of the references to colour in this figure legend, the reader is referred to the web version of this article.)

(Fig. 6 F G). Our data collectively illustrate that GIT1 modulates ERK1/2/SP1-dependent secretion of PDGF-BB in preosteoclasts.

4. Discussion

While early studies suggest that bone formation is mediated solely by osteoblasts, accumulating evidence indicates that the physiological function of osteogenesis is achieved by multiple tissue types in bone, including osteoclasts, vascular endothelium or autonomic and sensory nerves, which collectively contribute to a conducive milieu that facilitates bone formation [11,12,46,47]. In particular, TRAP+ cells (OCs and preosteoclasts) are proposed to not only play a role in bone resorption during bone formation but more importantly, function as metabolic secretions that interact with other cell types in the bone microenvironment [15,31,48]. However, this aspect of bone physiology remains poorly understood at present.

Recent studies have identified a specific $CD31^{hi}Emcn^{hi}$ vessel subtype regulated by PDGF-BB secreted by preosteoclasts and shown an association of abundance of this vessel subtype with bone formation [11,15]. Here, we utilized GIT1 KO mice showing significantly decreased bone formation as a study model to determine the mechanisms by which preosteoclasts regulate the $CD31^{hi}Emcn^{hi}$ vessel subtype in bone. In GIT1 KO mice, the $CD31^{hi}Emcn^{hi}$ vessel number was significantly decreased in bone marrow, accompanied by reduction of osteogenesis. Such phenotypes are also observed during fracture healing. PDGF-BB secretion by preosteoclasts was significantly decreased but no changes in the number of preosteoclasts were observed during induction in GIT1 KO mice, resulting in reduced bone formation and less $CD31^{hi}Emcn^{hi}$ vessels. As a shuttle protein, GIT1 mediates interactions with phosphorylated ERK1/2, in turn, leading to increased levels of nuclear SP1 that is critical for transcription of the PDGF-B gene in preosteoclasts [38]. Our findings highlight a novel biological function of GIT1 as an interacting partner with $CD31^{hi}Emcn^{hi}$ vessels in preosteoclasts.

Our group has documented important roles of GIT1 in pulmonary vascular development [21] and blood vessel formation during bone fracture healing [24]. In addition, previous research by our team showed that GIT1 is closely related to osteogenic bone mass [23]. Given the importance of GIT1 in angiogenesis, we were interested in ascertaining the relationship between GIT1 and $CD31^{hi}Emcn^{hi}$ vessels, a specific blood vessel type associated with osteogenesis. Immunofluorescence staining revealed lower levels of $CD31^{hi}Emcn^{hi}$ vessels under physiological conditions in GIT1 KO mice. In the fracture model, fracture healing was accompanied by a large number of $CD31^{hi}Emcn^{hi}$ vessels in GIT1 WT mice, which was significantly reduced in GIT1 KO mice. Here, we have demonstrated for the first time that GIT1 exerts a regulatory effect on osteogenesis-related $CD31^{hi}Emcn^{hi}$ vessels. Our novel findings explain how GIT1, a key regulatory protein of angiogenesis, can affect osteogenesis.

PDGF-BB is reported to induce proliferation, migration and angiogenesis of EPCs [13]. PDGF-BB secreted by preosteoclasts is considered to play a key role in bone modeling and remodeling through regulation of $CD31^{hi}Emcn^{hi}$ endothelium. Previously, we demonstrated that GIT1 is critical for activation of PLC-γ and ERK1/2 in endothelial cells and osteoblasts, leading to adjustment of VEGF expression in osteoblasts via the GIT1- ERK1/2 axis [49]. GIT1 additionally regulates osteoclast function and bone mass. Accordingly, we put forward the hypothesis that GIT1 is likely to regulate PDGF-BB secreted by preosteoclasts, ultimately affecting the distribution and quantity of $CD31^{hi}Emcn^{hi}$ vessels.

Flow cytometry analyses disclosed a normal number of preosteoclasts in GIT1 KO mice bone marrow. ELISA experiments further showed that knockout of GIT1 reduced PDGF-BB secretion by preosteoclasts, resulting in decreased EPC recruitment. Based on these findings, we suggest that GIT1 affects $CD31^{hi}Emcn^{hi}$ vessel levels through regulating the PDGF-BB secretory function of preosteoclasts. Vascular-related factors, such as VEGF, do not affect $CD31^{hi}Emcn^{hi}$ vessel formation [15]. However, the respective roles and associations of GIT1 with VEGF-induced angiogenesis and effects of PDGF-BB on $CD31^{hi}Emcn^{hi}$ vessels throughout bone modeling and remodeling require further exploration.

PDGF-BB secreted by preosteoclasts during bone formation provides an effective means to treat bone defects and is widely utilized for fracture healing and bone regeneration [50,51]. However, the molecular mechanism underlying sts-induced secretion of PDGF-BB remains unclear. The PDGF family of growth factors comprises five different disulfide-linked dimers made up of four different polypeptide chains encoded by different genes, including PDGF-BB consisting of two PDGF-B polypeptide chains [52]. Transcription of PDGF-BB is regulated by the transcription factor, specificity protein 1 (SP1) [38], which is activated through upstream phosphorylation of ERK1/2 [53]. GIT1, a shuttle protein, plays a critical role in the phosphorylation of ERK1/2 [45,49]. In this study, knockout of GIT1 in preosteoclasts induced suppression of downstream ERK1/2 phosphorylation, in turn, triggering a decrease in SP1 expression. ChIP and luciferase assays revealed that PDGF-B gene transcription was also reduced in GIT1 KO mice with decreased SP1 levels.

In our study, experiments were performed using GIT1 KO mice, whether the change of secretion of PDGF-BB in vivo was caused by the indirect effect of other after GIT1KO could not be fully explained. Previous studies have demonstrated that platetets, monocyte/macrophages, endothelial cells and vascular smooth muscle cells are the main source of PDGF-BB secretion [54,55]. Among them, monocyte/macrophages-induced osteoclasts and endothelial cells may play a key role in the formation of the $CD31^{hi}Emcn^{hi}$ vessel subtype in coupling osteogenesis. In this article, we have demonstrated that preosteoclasts secrete high levels of PDGF-BB whereas osteoclasts show significantly lower secretion of PDGF-BB in both GIT1 KO and WT mice (Fig. 4A,B). In addition, we found a low level of PDGF-BB secretion in endothelial cells and no significant difference in the amount of PDGF-BB secreted between GIT1 KO and WT mice (Supplementary Fig. 2). The effect of exact functions and mechanisms of GIT1 in preosteoclasts on the formation of $CD31^{hi}Emcn^{hi}$ vessel subtype requires further investigations using higher specificity monocytes/macrophages-CKO mice.

In sum, our collective findings demonstrate that GIT1 in pre-osteoclasts is involved in regulation of PDGF-BB secretion by modifying ERK1/2/SP1 signaling pathway. In addition, the influence of GIT1 on PDGF-BB regulates $CD31^{hi}Emcn^{hi}$ vessel and bone formation. GIT1 and its signaling partner(s) could potentially serve as pharmacological targets to treat delayed fracture healing and bone metabolic diseases.

Supplementary data to this article can be found online at https://doi.org/10.1016/j.bone.2019.03.006.

Acknowledgements

This study was funded by the National Natural Science Foundation of China (Grant Numbers 81772351, 81520108018, 81472080, 81772352, and 81401800) and the Nanjing Committee of Science and Technology (Grant Number 201505005).

Author contributions

G.Y. Yin and J. Fan designed and supervised this study; T. Xu, Y.J. Luo and FQ. Kong conducted experiments; B·Lv, SJ. Zhao and J. Chen contributed important intellectual content; T. Xu and Y.J. Luo wrote the manuscript;. All authors reviewed and approved the final version of this manuscript.

References

[1] E. Seeman, Bone modeling and remodeling, Crit. Rev. Eukaryot. Gene Expr. 19 (3) (2009) 219–233.
[2] A. Teti, Bone development: overview of bone cells and signaling, Curr. Osteoporos. Rep. 9 (4) (2011) 264–273.
[3] E.F. Eriksen, Cellular mechanisms of bone remodeling, Rev. Endocr. Metab. Disord. 11 (4) (2010) 219–227.
[4] M. Zaidi, Skeletal remodeling in health and disease, Nat. Med. 13 (7) (2007) 791–801.
[5] S. Portal-Nunez, D. Lozano, P. Esbrit, Role of angiogenesis on bone formation, Histol. Histopathol. 27 (5) (2012) 559–566.
[6] M.L. Brandi, P. Collin-Osdoby, Vascular biology and the skeleton, J. Bone Miner. Res. Off. J. Am. Soc. Bone Miner. Res. 21 (2) (2006) 183–192.
[7] S.M. Chim, J. Tickner, S.T. Chow, V. Kuek, B. Guo, G. Zhang, V. Rosen, W. Erber, J. Xu, Angiogenic factors in bone local environment, Cytokine Growth Factor Rev. 24 (3) (2013) 297–310.
[8] A.M. Parfitt, The mechanism of coupling: a role for the vasculature, Bone 26 (4) (2000) 319–323.
[9] P. Carmeliet, R.K. Jain, Molecular mechanisms and clinical applications of angiogenesis, Nature 473 (7347) (2011) 298–307.
[10] W.C. Chen, T.S. Park, I.R. Murray, L. Zimmerlin, L. Lazzari, J. Huard, B. Peault, Cellular kinetics of perivascular MSC precursors, Stem Cells Int. 2013 (2013) 983059.
[11] A.P. Kusumbe, S.K. Ramasamy, R.H. Adams, Coupling of angiogenesis and osteogenesis by a specific vessel subtype in bone, Nature 507 (7492) (2014) 323–328.
[12] S.K. Ramasamy, A.P. Kusumbe, L. Wang, R.H. Adams, Endothelial notch activity promotes angiogenesis and osteogenesis in bone, Nature 507 (7492) (2014) 376–380.
[13] H. Wang, Y. Yin, W. Li, X. Zhao, Y. Yu, J. Zhu, Z. Qin, Q. Wang, K. Wang, W. Lu, J. Liu, L. Huang, Over-expression of PDGFR-beta promotes PDGF-induced proliferation, migration, and angiogenesis of EPCs through PI3K/Akt signaling pathway, PLoS One 7 (2) (2012) e30503.
[14] J. Fiedler, N. Etzel, R.E. Brenner, To go or not to go: migration of human mesenchymal progenitor cells stimulated by isoforms of PDGF, J. Cell. Biochem. 93 (5) (2004) 990–998.
[15] H. Xie, Z. Cui, L. Wang, Z. Xia, Y. Hu, L. Xian, C. Li, L. Xie, J. Crane, M. Wan, G. Zhen, Q. Bian, B. Yu, W. Chang, T. Qiu, M. Pickarski, L.T. Duong, J.J. Windle, X. Luo, E. Liao, X. Cao, PDGF-BB secreted by preosteoclasts induces angiogenesis during coupling with osteogenesis, Nat. Med. 20 (11) (2014) 1270–1278.
[16] A. Del Fattore, A. Teti, N. Rucci, Bone cells and the mechanisms of bone remodelling, Front. Biosci. 4 (2012) 2302–2321.
[17] A. Claing, S.J. Perry, M. Achiriloaie, J.K. Walker, J.P. Albanesi, R.J. Lefkowitz, R.T. Premont, Multiple endocytic pathways of G protein-coupled receptors delineated by GIT1 sensitivity, Proc. Natl. Acad. Sci. U. S. A. 97 (3) (2000) 1119–1124.
[18] R.T. Premont, A. Claing, N. Vitale, J.L. Freeman, J.A. Pitcher, W.A. Patton, J. Moss, M. Vaughan, R.J. Lefkowitz, beta2-adrenergic receptor regulation by GIT1, a G protein-coupled receptor kinase-associated ADP ribosylation factor GTPase-activating protein, Proc. Natl. Acad. Sci. U. S. A. 95 (24) (1998) 14082–14087.
[19] K. Natarajan, G. Yin, B.C. Berk, Scaffolds direct Src-specific signaling in response to angiotensin II: new roles for Cas and GIT1, Mol. Pharmacol. 65 (4) (2004) 822–825.
[20] R.J. Hoefen, B.C. Berk, The multifunctional GIT family of proteins, J. Cell Sci. 119 (Pt 8) (2006) 1469–1475.
[21] J. Pang, R. Hoefen, G.S. Pryhuber, J. Wang, G. Yin, R.J. White, X. Xu, M.R. O'Dell, A. Mohan, H. Michaloski, M.P. Massett, C. Yan, B.C. Berk, G-protein-coupled receptor kinase interacting protein-1 is required for pulmonary vascular development, Circulation 119 (11) (2009) 1524–1532.
[22] J. Wang, Y. Taba, J. Pang, G. Yin, C. Yan, B.C. Berk, GIT1 mediates VEGF-induced podosome formation in endothelial cells: critical role for PLCgamma, Arterioscler. Thromb. Vasc. Biol. 29 (2) (2009) 202–208.
[23] P. Menon, G. Yin, E.M. Smolock, M.J. Zuscik, C. Yan, B.C. Berk, GPCR kinase 2 interacting protein 1 (GIT1) regulates osteoclast function and bone mass, J. Cell. Physiol. 225 (3) (2010) 777–785.
[24] G. Yin, T.J. Sheu, P. Menon, J. Pang, H.C. Ho, S. Shi, C. Xie, E. Smolock, C. Yan, M.J. Zuscik, B.C. Berk, Impaired angiogenesis during fracture healing in GPCR kinase 2 interacting protein-1 (GIT1) knock out mice, PLoS One 9 (2) (2014) e89127.
[25] L. Xian, X. Wu, L. Pang, M. Lou, C.J. Rosen, T. Qiu, J. Crane, F. Frassica, L. Zhang, J.P. Rodriguez, J. Xiaofeng, Y. Shoshana, X. Shouhong, E. Argiris, W. Mei, C. Xu, Matrix IGF-1 maintains bone mass by activation of mTOR in mesenchymal stem cells, Nat. Med. 18 (7) (2012) 1095–1101.
[26] X. Wu, L. Pang, W. Lei, W. Lu, J. Li, Z. Li, F.J. Frassica, X. Chen, M. Wan, X. Cao, Inhibition of Sca-1-positive skeletal stem cell recruitment by alendronate blunts the anabolic effects of parathyroid hormone on bone remodeling, Cell Stem Cell 7 (5) (2010) 571–580.
[27] G. Zhen, C. Wen, X. Jia, Y. Li, J.L. Crane, S.C. Mears, F.B. Askin, F.J. Frassica, W. Chang, J. Yao, J.A. Carrino, A. Cosgarea, D. Artemov, Q. Chen, Z. Zhao, X. Zhou, L. Riley, P. Sponseller, M. Wan, W.W. Lu, X. Cao, Inhibition of TGF-beta signaling in mesenchymal stem cells of subchondral bone attenuates osteoarthritis, Nat. Med. 19 (6) (2013) 704–712.
[28] C. Xie, B. Liang, M. Xue, A.S. Lin, A. Loiselle, E.M. Schwarz, R.E. Guldberg, R.J. O'Keefe, X. Zhang, Rescue of impaired fracture healing in COX-2−/− mice via activation of prostaglandin E2 receptor subtype 4, Am. J. Pathol. 175 (2) (2009) 772–785.
[29] X. Zhang, C. Xie, A.S. Lin, H. Ito, H. Awad, J.R. Lieberman, P.T. Rubery, E.M. Schwarz, R.J. O'Keefe, R.E. Guldberg, Periosteal progenitor cell fate in segmental cortical bone graft transplantations: implications for functional tissue engineering, J. Bone Miner. Res. Off. J. Am. Soc. Bone Miner. Res. 20 (12) (2005) 2124–2137.
[30] R.S. Dhillon, C. Xie, W. Tyler, L.M. Calvi, H.A. Awad, M.J. Zuscik, R.J. O'Keefe, E.M. Schwarz, PTH-enhanced structural allograft healing is associated with decreased angiopoietin-2-mediated arteriogenesis, mast cell accumulation, and fibrosis, J. Bone Miner. Res. Off. J. Am. Soc. Bone Miner. Res. 28 (3) (2013) 586–597.
[31] R. Xu, A. Yallowitz, A. Qin, Z. Wu, D.Y. Shin, J.M. Kim, S. Debnath, G. Ji, M.P. Bostrom, X. Yang, C. Zhang, H. Dong, P. Kermani, S. Lalani, N. Li, Y. Liu, M.G. Poulos, A. Wach, Y. Zhang, K. Inoue, A. Di Lorenzo, B. Zhao, J.M. Butler, J.H. Shim, L.H. Glimcher, M.B. Greenblatt, Targeting skeletal endothelium to ameliorate bone loss, Nat. Med. 24 (6) (2018) 823–833.
[32] T.A. Einhorn, The cell and molecular biology of fracture healing, Clin. Orthop. Relat. Res. (355 Suppl) (1998) S7–21.
[33] T. Fukuda, S. Takeda, R. Xu, H. Ochi, S. Sunamura, T. Sato, S. Shibata, Y. Yoshida, Z. Gu, A. Kimura, C. Ma, C. Xu, W. Bando, K. Fujita, K. Shinomiya, T. Hirai, Y. Asou, M. Enomoto, H. Okano, A. Okawa, H. Itoh, Sema3A regulates bone-mass accrual through sensory innervations, Nature 497 (7450) (2013) 490–493.
[34] R. Xu, C. Zhang, D.Y. Shin, J.M. Kim, S. Lalani, N. Li, Y.S. Yang, Y. Liu, M. Eiseman, R.J. Davis, J.H. Shim, M.B. Greenblatt, C-Jun N-terminal kinases (JNKs) are critical mediators of osteoblast activity in vivo, J. Bone Miner. Res. Off. J. Am. Soc. Bone Miner. Res. 32 (9) (2017) 1811–1815.
[35] K. Tanaka, M. Hashizume, M. Mihara, H. Yoshida, M. Suzuki, Y. Matsumoto, Anti-interleukin-6 receptor antibody prevents systemic bone mass loss via reducing the number of osteoclast precursors in bone marrow in a collagen-induced arthritis model, Clin. Exp. Immunol. 175 (2) (2014) 172–180.
[36] J. Zhang, J. Guan, X. Niu, G. Hu, S. Guo, Q. Li, Z. Xie, C. Zhang, Y. Wang, Exosomes released from human induced pluripotent stem cells-derived MSCs facilitate cutaneous wound healing by promoting collagen synthesis and angiogenesis, J. Transl. Med. 13 (2015) 49.
[37] L.A. Rafty, L.M. Khachigian, von Hippel-Lindau tumor suppressor protein represses platelet-derived growth factor B-chain gene expression via the Sp1 binding element in the proximal PDGF-B promoter, J. Cell. Biochem. 85 (3) (2002) 490–495.
[38] L.A. Rafty, L.M. Khachigian, Sp1 phosphorylation regulates inducible expression of platelet-derived growth factor B-chain gene via atypical protein kinase C-zeta, Nucleic Acids Res. 29 (5) (2001) 1027–1033.
[39] R. Faccio, S.L. Teitelbaum, K. Fujikawa, J. Chappel, A. Zallone, V.L. Tybulewicz, F.P. Ross, W. Swat, Vav3 regulates osteoclast function and bone mass, Nat. Med. 11 (3) (2005) 284–290.
[40] J. Haendeler, G. Yin, Y. Hojo, Y. Saito, M. Melaragno, C. Yan, V.K. Sharma, M. Heller, R. Aebersold, B.C. Berk, GIT1 mediates Src-dependent activation of phospholipase Cgamma by angiotensin II and epidermal growth factor, J. Biol. Chem. 278 (50) (2003) 49936–49944.
[41] R. Marsell, T.A. Einhorn, The biology of fracture healing, Injury 42 (6) (2011) 551–555.
[42] J. Glowacki, Angiogenesis in fracture repair, Clin. Orthop. Relat. Res. 355 (Suppl) (1998) S82–S89.
[43] B.F. Boyce, L. Xing, Functions of RANKL/RANK/OPG in bone modeling and remodeling, Arch. Biochem. Biophys. 473 (2) (2008) 139–146.
[44] S.Y. Gao, G.S. Zheng, L. Wang, Y.J. Liang, S.E. Zhang, X.M. Lao, K. Li, G.Q. Liao, Zoledronate suppressed angiogenesis and osteogenesis by inhibiting osteoclasts formation and secretion of PDGF-BB, PLoS One 12 (6) (2017) e0179248.
[45] G. Yin, Q. Zheng, C. Yan, B.C. Berk, GIT1 is a scaffold for ERK1/2 activation in focal adhesions, J. Biol. Chem. 280 (30) (2005) 27705–27712.
[46] Y. Zhang, J. Xu, Y.C. Ruan, M.K. Yu, M. O'Laughlin, H. Wise, D. Chen, L. Tian,

D. Shi, J. Wang, S. Chen, J.Q. Feng, D.H. Chow, X. Xie, L. Zheng, L. Huang, S. Huang, K. Leung, N. Lu, L. Zhao, H. Li, D. Zhao, X. Guo, K. Chan, F. Witte, H.C. Chan, Y. Zheng, L. Qin, Implant-derived magnesium induces local neuronal production of CGRP to improve bone-fracture healing in rats, Nat. Med. 22 (10) (2016) 1160–1169.

[47] R. Xu, Semaphorin 3A: a new player in bone remodeling, Cell Adhes. Migr. 8 (1) (2014) 5–10.

[48] D. Li, J. Liu, B. Guo, C. Liang, L. Dang, C. Lu, X. He, H.Y. Cheung, L. Xu, C. Lu, B. He, B. Liu, A.B. Shaikh, F. Li, L. Wang, Z. Yang, D.W. Au, S. Peng, Z. Zhang, B.T. Zhang, X. Pan, A. Qian, P. Shang, L. Xiao, B. Jiang, C.K. Wong, J. Xu, Z. Bian, Z. Liang, D.A. Guo, H. Zhu, W. Tan, A. Lu, G. Zhang, Osteoclast-derived exosomal miR-214-3p inhibits osteoblastic bone formation, Nat. Commun. 7 (2016) 10872.

[49] Z. Rui, X. Li, J. Fan, Y. Ren, Y. Yuan, Z. Hua, N. Zhang, G. Yin, GIT1Y321 phosphorylation is required for ERK1/2- and PDGF-dependent VEGF secretion from osteoblasts to promote angiogenesis and bone healing, Int. J. Mol. Med. 30 (4) (2012) 819–825.

[50] G.E. Friedlaender, S. Lin, L.A. Solchaga, L.B. Snel, S.E. Lynch, The role of recombinant human platelet-derived growth factor-BB (rhPDGF-BB) in orthopaedic bone repair and regeneration, Curr. Pharm. Des. 19 (19) (2013) 3384–3390.

[51] S. Graham, A. Leonidou, M. Lester, M. Heliotis, A. Mantalaris, E. Tsiridis, Investigating the role of PDGF as a potential drug therapy in bone formation and fracture healing, Expert Opin. Investig. Drugs 18 (11) (2009) 1633–1654.

[52] L. Fredriksson, H. Li, U. Eriksson, The PDGF family: four gene products form five dimeric isoforms, Cytokine Growth Factor Rev. 15 (4) (2004) 197–204.

[53] T. Lin, Y. Chen, Z. Ding, G. Luo, J. Liu, J. Shen, Novel insights into the synergistic interaction of a thioredoxin reductase inhibitor and TRAIL: the activation of the ASK1-ERK-Sp1 pathway, PLoS One 8 (5) (2013) e63966.

[54] A.D. Hughes, G.F. Clunn, J. Refson, C. Demoliou-Mason, Platelet-derived growth factor (PDGF): actions and mechanisms in vascular smooth muscle, Gen. Pharmacol. 27 (7) (1996) 1079–1089.

[55] R. Ross, Platelet-derived growth factor, Annu. Rev. Med. 38 (1987) 71–79.